Proton-transfer kinetics at liquid-liquid interfaces

Nick D'Antona[1,5], Nadia Barnard[1], Shane Ardo[2], Yixian Wang[3], Yogesh Surendranath[4], Paul Kempler[1]*, Shannon Boettcher[1,5,6]*

[1] *Department of Chemistry and Biochemistry and the Oregon Center for Electrochemistry, University of Oregon, Eugene, OR, USA.*

[2] *Department of Chemistry, University of California, Irvine, Irvine, CA, USA.*

[3] *Department of Chemistry, California State University, Los Angeles, Los Angeles, CA, USA.*

[4] *Department of Chemistry, Massachusetts Institute of Technology, Cambridge, MA, USA.*

[5] *Department of Chemical & Biomolecular Engineering and Department of Chemistry, University of California, Berkeley*

[6] *Energy Storage and Distributed Resources Division, Lawrence Berkeley National Laboratory, Berkeley, CA 94720, United States*

Abstract

Proton transfer at electrochemical interfaces is fundamentally important for many areas of science and technology, yet kinetic measurements of this elementary step are often convoluted by inhomogeneous electrode surface structures. We show that facilitated proton transfer at the interface between two immiscible electrolyte solutions (ITIES) can serve as a model system to study proton transfer kinetics in the absence of defects found at solid|electrolyte interfaces. Diffusion-controlled micropipette voltammetry revealed that 2,6-diphenylpyridine (DPP) facilitated interfacial proton-transfer across the HCl(aq)|Trifluorotoluene interface and voltammetry at nanopipette-supported interfaces yielded activation-controlled ion transfer currents. Fitting quasireversible voltammograms to a mixed diffusive-kinetic model allow for the extraction of kinetic parameters k^0 and α, which were equal to 3.0 +/- 1.8 cm/s and 0.3 +/- 0.2, respectively for DPP facilitated proton transfer. Finite element simulations highlighted regimes of direct proton transfer and sequential proton transfer, where the current divided between these two possible pathways was shown to favor direct PT when the neutral partitioning step DPP(org)→ DPP(aq) was rate determining. Understanding the kinetics of ion transfer at the ITIES will be

important in the development of general theories of ion transfer in electrochemical science and technology.

Introduction

Ion transfer – that is the movement of an ion across a phase boundary along with modulation of the ion's solvation shell – is a fundamental process across many fields, from biology to electrochemical technology, whose kinetics govern many different functions. The mechanisms of ion transfer, particularly a chemical understanding of the reaction pathway(s), however, are poorly understood. The kinetics of ion transfer are often implicitly overlooked when electrochemical reaction rates are analyzed, for example, in the framework of electron-transfer models such as with the Marcus or Butler-Volmer formulations. For reactions where reactive ions must cross the electrochemical double layer – examples being desolvation and ion adsorption during hydrogen evolution[1], metal corrosion,[2, 3] or Na/Li-ion insertion[4, 5] – electron transfer is unlikely to be the rate-controlling step. In these examples, interfacial ion transfer is the charge-transfer step that consumes the majority of the kinetic overpotential.[3] Yet for many such reactions, theories that were developed for simple electron transfer are applied to analyze the kinetics and mechanism of interfacial ionic processes.[4, 6] Improved kinetic models for reactions where ion transfer is rate limiting can support the design of new catalysts to accelerate these processes. Significant progress in this area has been made by Bazant for classical electrochemical coupled ion-electron transfer[6] and Hynes for the fully quantum mechanical coupled proton-electron transfer,[7, 8] yet there are few experimental platforms to straightforwardly test the predictions from these theories.

The interface between two immiscible electrolyte solutions (ITIES) allows for the study of interfacial ion-transfer processes in the absence of interfacial electron transfer. When no common ions exist between the two electrolytes, the interface is polarizable, that is, an electrochemical double layer can be formed under voltage control and ion-transfer rates can be studied as a function of electrochemical driving force. Crucially, the ITIES interface lacks the structural defects present at crystalline solid|liquid interfaces, such as terraces, kinks, and step edges, which are thought to have a disproportionate effect on ion-transfer

rates at solid surfaces.[9-11] In analogy, liquid-mercury|electrolyte interfaces have been used widely to develop our understanding of electron transfer and the structure of the double-layer.[12]

Here we report kinetic studies of facilitated proton-transfer (PT) reactions at the ITIES, given the broad importance of PT in water electrolysis,[13] CO_2 reduction,[14] and enzyme catalyzed reactions in biology.[15] There have been related efforts to develop theories of proton-coupled electron transfer (PCET) at interfaces,[16-18] and experiments to understand driving-force dependence of PCET reactions for different catalysts and electrolytes.[19, 20] PT is most often studied indirectly, for example in the context of the hydrogen evolution reaction (HER), where the rate of PT to the electrode surface can be inferred from the overall HER rate under certain experimental conditions.[21, 22] Well-defined hydrogen underpotential deposition (H-UPD) waves have been studied at single-crystal electrodes, which restricts the measured kinetics to a single, self-limited adsorption/desorption step.[1] Yet, in either of these measurements, the distribution and density of structural defects on the surface are not known, and thus the measured rate constant represents an ensemble average of activation barriers across the surface for these distribution of heterogenous sites.

PT at the ITIES, where aqueous protons, H^+(aq), are transferred to a non-aqueous basic, B(org), acceptor species (Eq 1)

$$H^+(aq) + B(org) \rightarrow BH^+(org) \qquad (1)$$

in principle allows for the rate of PT across a polarized interface to be measured in the absence of any well-defined surface structure. In this system, there is no preferred proton adsorption site related to surface morphology. The non-aqueous basic proton-accepting molecule lowers the standard potential for the transfer of the proton, enabling the study of proton-transfer rates without the convoluting current of background electrolyte ion transfer (**Figure 1**). Of particular interest is the standard rate constant k^0 for this reaction, as it measures the facility of the proton-transfer reaction at equilibrium and standard-state conditions. Tracking changes to k^0 as a function of solvent properties such as viscosity or dielectric constant would be important for testing hypotheses about the molecular details that gate ion-transfer rates.

When an ionizable solute, B(org), is present in an ITIES electrochemical cell, it may spontaneously partition between aqueous and organic phases according to its aqueous acid dissociation constant K_a, partition coefficient P, and the pH of the aqueous phase, complicating kinetic analysis. When neutral and ionized forms of B(org) are distributed between the two phases, the application of a Galvani potential difference $\Delta_o^w\phi$ across the interface may drive the *i)* direct transfer of H+(aq) to B(org) across the phase boundary, *ii)* transfer of the conjugate acid BH^+(aq) (as a minority species previously partitioned to the organic phase), *iii)* shuttling via an interfacial-sequential pathway, or all processes simultaneously (**Figure 1**). Since there are multiple possible processes responsible for the observed current, it is important understand if and how the measured k^0 can be understood in terms of molecular interfacial proton-transfer kinetics and mechanisms.

Previously, ionic partition diagrams have been developed to assess the speciation of dissolved B as a function of pH and $\Delta_o^w\phi$, where the boundaries of the predominance areas can be calculated from the pK_a, partition coefficient P, and the formal potential for ion transfer $\Delta_o^w\phi^{0\prime}$.[23-25] The boundary lines can also be determined experimentally by measuring the change in the cyclic-voltammogram halfwave potential with a change in the pH of the aqueous phase. At the boundary between two different predominance areas in an ionic partition diagram, the thermodynamically favored phase of B may change, and from this one can infer whether the cation being transferred is the conjugate acid BH^+, or H^+ facilitated by diffusion of B(org) to the interface, as $\Delta_o^w\phi$ is changed from negative to positive with respect to a boundary line.

However, these thermodynamic diagrams are insufficient to distinguish between the case where a H^+ is transferred from hydronium to the B(org) in the organic phase *across* the liquid-liquid interface, and where H^+ is transferred from hydronium to an intermediate B(aq) *within* the aqueous phase to produce interfacial HB^+(aq). The HB^+(aq) intermediate would then be subjected to $\Delta_o^w\phi$ and transferred across the interface to carry the observed current. A depiction of the possible pathways for facilitated proton transfer is shown in **Figure 1**. While it is expected that highly lipophilic (large partition coefficient) bases would transfer a proton via the interfacial-direct mechanism, and mildly lipophilic bases via the interfacial-indirect

mechanism, a quantitative relationship between thermodynamic and kinetic variables has not yet been developed to the best of our knowledge.

Measurements of k^0 for facilitated ion transfer at the ITIES are further complicated by the absence of a well-defined equilibrium potential about which rate-driving force measurements should be made.[26-28] This absence is because, in a typical facilitated proton-transfer experiment, only the neutral proton acceptor is added to the organic phase—a situation analogous to only adding the "reduced species" of a redox couple to the electrolyte in a voltammetry experiment. In the absence of a well-defined equilibrium potential, the formal potential for ion transfer $\Delta_o^w\phi^{0\prime}$ must be known to accurately calculate the driving force for facilitated ion transfer. Most commonly this value is not known *a priori* and must be included as a free fit-parameter along with $k^0$and α in a mixed diffusive-kinetic model (to fit a steady-state voltammogram), introducing additional uncertainty in the desired kinetic parameters k^0 and α. Together, the uncertainty in the interfacial pathway for facilitated proton transfer and the absence of a well-defined equilibrium potential warrants caution in the interpretation of previously reported k^0 values for facilitated proton transfer.[29, 30]

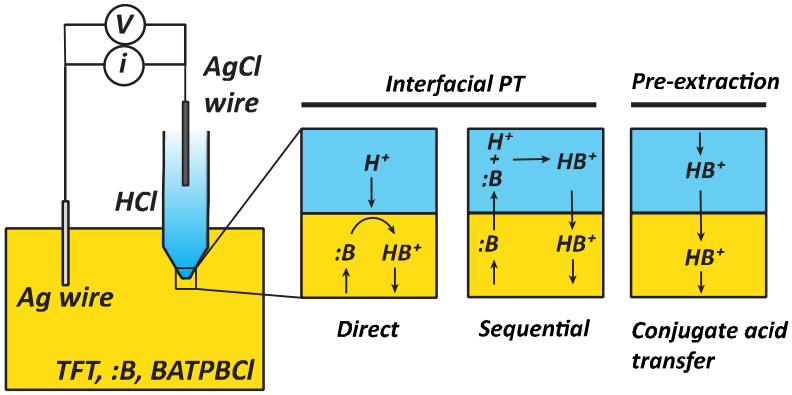

Figure 1 | Scheme of electrochemical cell used for measurements of facilitated PT. Laser-pulled quartz pipettes with diameters ca. 2-10 µm were filled with aqueous HCl and submerged in an immiscible nonaqueous electrolyte (TFT containing 5 mM supporting electrolyte) to form a micro liquid-liquid interface at the tip. Nanoamp-scale currents are observed when a hydrophobic organic base is initially added to the nonaqueous electrolyte, and a potential difference is applied between the two phases. Interfacial-direct PT is the fully coupled reaction limited to the interfacial region when a proton would be transferred from H_3O^+ at the aqueous|organic interface to B(org). Interfacial-sequential transfer is a nonequilibrium process where neutral phase transfer and protonation within the aqueous phase occur prior to the electrochemical step. Highly lipophilic bases will spontaneously partition between the two phases and result in a bulk concentration of conjugate acid species at equilibrium capable of carrying current at positive overpotentials. Distinguishing

between, and studying the kinetics of, the various pathways provides insight into what controls the rate of ion transfer broadly.

In this work we use the ITIES as a model system for the study of interfacial proton transfer in the absence of surface defects common to all solid electrode-electrolyte interfaces, with special attention to the issue of interpreting the standard rate constant k^0. We first compare two different proton acceptors, 2,6-diphenylpyridine (log(*P*) = 5) and 9-methylacridine (log(*P*) = 3.5), in a single diffusion-limited micropipette voltammetry experiment to explore the distinction between pre-extraction and interfacial proton-transfer pathways and designate a proton acceptor to be suitable for the use as a model system. The asymmetric geometry of the conical pipette leads to different diffusion profiles, which in turn allows us to assign a dominant pathway for proton-transfer for each base from the standpoint of diffusion-limited voltammetry. We determined that 2,6-diphenylpyridine does not pre-extract to an appreciable extent at an aqueous electrolyte pH of 1, whereas 9-methylacridine partitions itself significantly before the start of the experiment such that most of the observed current is carried by $9MAH^+$. Following this experiment, the conjugate acid salt of 2,6-diphenylpyridine, (2,6-diphenylpyridinium tetrakis(3,5-bis(trifluoromethyl)phenyl)borate), was synthesized for use in a "common-ion" nanopipette voltammetry experiment, allowing for the measurement of k^0 about a well-defined equilibrium potential for the first time. From this measurement, we obtained values k^0 and α equal to 3.0 +/- 1.8 cm/s and 0.3 +/- 0.2, respectively. We consider the possibility that an interfacial proton acceptor may still indirectly carry the proton across the interface via a neutral aqueous intermediate, and use multiphysics finite-element simulations to quantitatively assess the possible contributions from parallel direct and sequential proton-transfer pathways. With these simulation results, we found that the interfacial-direct pathway dominates the current response for a wide range of possible exchange current densities, overpotentials, and partitioning rate constants.

With the broad goal of understanding proton transfer kinetics at the ITIES, we have shown via diffusion-limited micropipette voltammetry experiments that a lipophilic basic molecule may

spontaneously partition itself such that most of the observed current is carried by its conjugate acid sourced from the bulk aqueous electrolyte. We found this to be the case with 9MA as a lipophilic base and argued that any lipophilic base proceeding by this pathway for proton transfer would be unsuitable for the further study of proton-transfer kinetics. In contrast, DPP facilitated proton-transfer in micropipette electrochemical cells was found to be consistent with the expected voltammogram of interfacial proton transfer pathway, however short-lived intermediates B(aq) and HB+(aq) close to the liquid-liquid interface ultimately could not be ruled out from the experimental data. We showed with Multiphysics simulations that physically reasonable values of a neutral partitioning rate constant ($k_{f,PhT}$) would lead to the suppression of the interfacial-sequential pathway over a wide range of exchange current densities considered for direct and sequential proton transfer pathways, resulting in increased confidence that the measured standard rate constant in this work is representative of interfacial direct proton transfer and not one of the other pathways considered.

Results and Discussion

Characterizing facilitated proton-transfer reaction pathways. Facilitated PT rates were measured at the water|trifluorotoluene (TFT) interface with the working electrode immersed in the aqueous phase, such that positive current could be assigned to either cation transfer from the aqueous to organic phase *or* anion transfer in the reverse direction. Because the polarization resistance of the cell is dominated by the micrometer-scale liquid|liquid interface supported at the pipette tip, the potential drop between the aqueous and nonaqueous electrodes is fully assigned to the potential drop at the water|TFT interface, $\Delta_o^w\phi$. **Figure 2** shows the polarization response when 0.5 mM of either 2,6-diphenylpyridine (DPP) or 9-methylacridine (9MA) is added to the TFT electrolyte. The negative shift in the current onset is due to the facilitated transfer of a proton from the acidic aqueous phase by one of the proposed pathways shown in **Figure 1**. In the absence of either of these basic

molecules, proton-transfer current is convoluted with the organic-to-aqueous phase transfer of $TPBCl^-$ at cell potentials > 0.3 V.

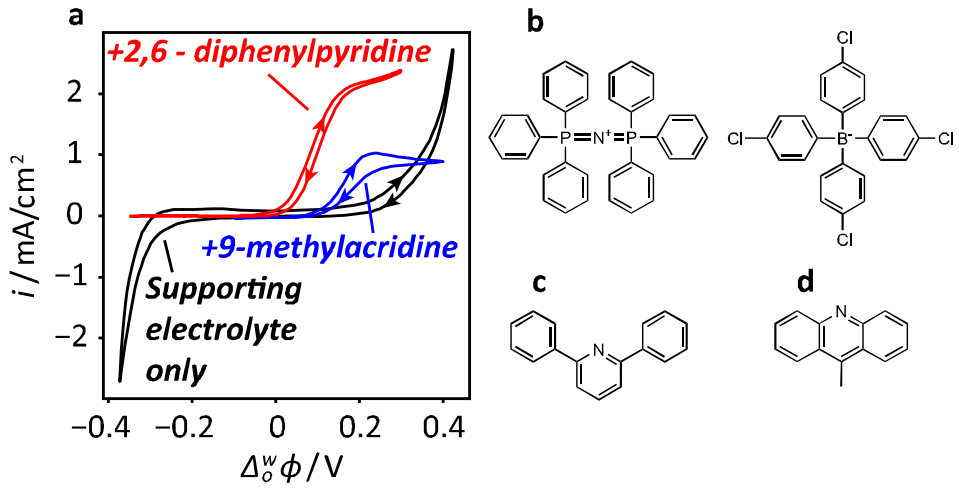

Figure 2 | Effect of adding organic bases to nonaqueous electrolyte. (a) Cyclic voltammograms of ion transfer at the ITIES with only 5 mM supporting electrolyte in the nonaqueous phase (black trace), supporting electrolyte plus 0.5 mM of 9-methylacridine (blue trace), and supporting electrolyte plus 0.5 mM 2,6-diphenylpyridine (red trace). Each experiment was performed in a separate electrochemical cell, where the organic reference electrode potentials are similar but subject to small changes between experiments, thus differences in potential for current onset only serve as a qualitative comparison between experiments. Skeletal structures of species indicated in figure inset, where BATPBCl is the identity of the supporting electrolyte (b), 2,6-diphenylpyridine (c), 9-methylacridine (d).

To distinguish between pre-extraction and interfacial pathways, cyclic voltammograms of DPP and 9MA were collected in micropipette (radii ~4 μm) electrochemical cells at increasing scan rates. Initially, the organic phase, and by extension the phase in which the base is originally present, was positioned inside the pipette (**Figure 3a**) and the corresponding CVs are shown in **Figure 3b,c**. The CV for DPP facilitated proton-transfer exhibited a positive and negative peak positioned at 0.5 and 0.4 V in the cell used for that experiment, respectively, both of which grew with increasing scan rates from 50 - 400 mV/s. This is qualitatively different from the case of 9MA facilitated proton-transfer, where a positive limiting-current plateau was observed on the positive sweep and a negative peak was observed around 0.1 V (that also grew with increasing scan rates).

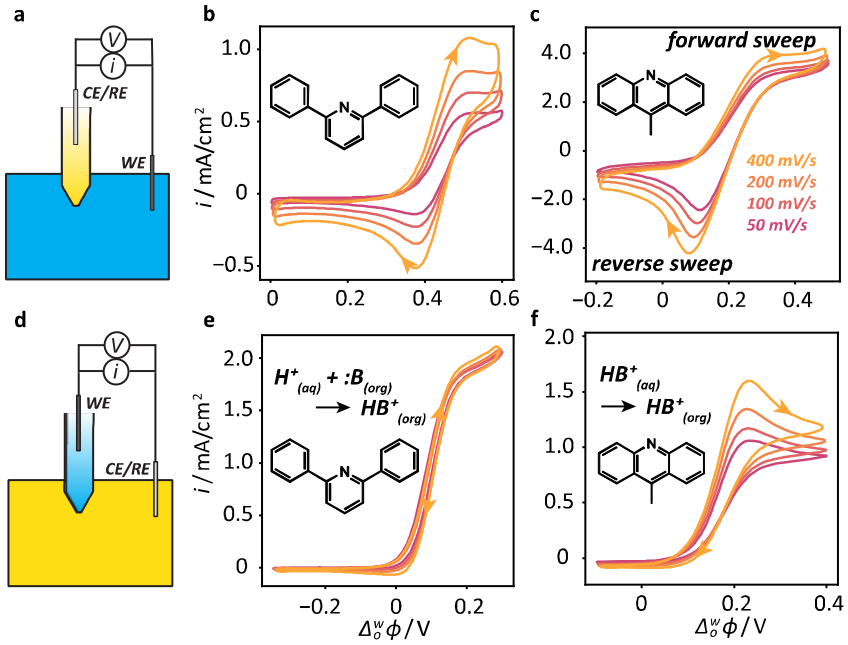

Figure 3 | Cyclic voltammograms of PT facilitated by 2,6-diphenylpyridine (b, e) and 9-methylacridine (c, f). Bases are initially present in the organic phase at 0.5 mM with 5 mM organic supporting electrolyte before equilibrating with the 100 mM HCl aqueous phase ex-situ in equal volumes. The position of electrolytes for each row are indicated by the schematics on the left (**a, d**), where blue corresponds to the aqueous phase and gold corresponds to the organic phase. Scan rates are color consistent with all traces. The presence of asymmetric diffusion peaks in 9-methylacridine facilitated PT is consistent with indirect conjugate acid PT, whereas symmetric diffusion peaks in 2,6-diphenylpyridine facilitated PT is due to direct interfacial PT.

The above behavior can be rationalized by considering the asymmetric geometry of the pipette and the different diffusion profiles that would arise from species transport inside or outside the pipette. Given the confined space within the pipette relative to the pipette orifice, an inner diffusing species should follow roughly semi-infinite linear diffusion giving peaked-current behavior in the cyclic voltammetry analysis (as is typically observed for a freely diffusing redox couple in an unstirred solution at a planar electrode). In contrast, the diffusion boundary layer outside of the pipette is allowed to expand radially in all directions and has dimensions comparable to the dimensions of the micropipette, leading to a hemispherical diffusion profile and a concomitant steady-state current (as is typically observed for redox at an analogous solid nano- or micro-electrode). Thus, observation of positive and negative peaks in the DPP-facilitated proton-transfer voltammograms suggests that DPP is diffusing to and from the interface *only in the organic phase.* This

interpretation is further supported by the data in **Figure 3e,** where the organic phase containing DPP is positioned on the outside of the pipette. Only steady-state current was observed in the scan-rate range tested because DPP is now diffusing to and from the interface from the outside of the pipette, where a hemispherical diffusion profile is formed.

With this information, the asymmetric CV seen in 9MA facilitated proton-transfer (**Figure 3c**), is consistent with 9MA existing primarily as its conjugate acid form ($9MAH^+$) in the acidic aqueous phase before the experiment is started. With the application of more positive potential, $9MAH^+$ is driven into the pipette from the outer aqueous phase on the forward sweep, and then expelled from the inner organic phase on the reverse sweep, leading to steady-state and peak-shaped current profiles, respectively, on the different sweep directions. Switching the positions of the two phases (inside pipette versus outside, **Figure 3f**) produced a CV with peak-shaped current on the forward sweep and a steady-state current on the reverse sweep, again consistent with the model that $9MAH^+$ is initially present in the acidic aqueous and transferred to the organic phase. This type of reasoning has been used previously to infer pathways of facilitated ion transfer.[31] Together, these results illustrate that DPP undergoes an interfacial facilitated proton-transfer mechanism pathway and 9MA follows the pre-extraction pathway with pH 1 aqueous electrolyte. It does not, however, prove that the transfer is direct, and other possible mechanisms are discussed below. It is possible that intermediate reactions steps at the interface happen in series with diffusion of the acceptor species to the interface (See **Figure 1**, interfacial-sequential pathway). If the kinetics of these intermediate reaction steps are fast relative to diffusion, then a diffusion limited voltammetry experiment cannot distinguish between interfacial-direct and interfacial-sequential mechanisms. It is, however, useful for illustrating the complexity of facilitated ion transfer reactions and rapid screening for lipophilic bases that significantly pre-extract for a given aqueous pH condition. The question of which interfacial pathway is operative will be discussed more below.

Multiphysics finite-element simulations of interfacial kinetics and transport. COMSOL Multiphysics was used to generate a model where the cone of a nanopipette containing 100 mM H^+ is in

contact with the outer electrolyte containing 0.5 mM DPP and $DPPH^+$. For simplicity, migration is not included in the model and transport through the cell was by diffusion only. Convection is also not expected to play a major role in these experiments. At the tip of the pipette, where the liquid-liquid interface is modeled to be, a square-scheme mechanism for facilitated ion transfer is considered (**Figure 4c**). The top edge of the square scheme represents the interfacial-direct mechanism, where aqueous protons react directly with DPP at the position of the simulated liquid-liquid interface. The other 3 legs of the square scheme make up the interfacial-sequential mechanism, which has two preceding chemical steps and a final electrochemical step. Specifically, a chemical step consisting of a heterogeneous organic-to-aqueous phase-transfer of DPP with equilibrium constant equal to the partition coefficient *P*, a chemical step consisting of a homogeneous acid-base reaction on the aqueous side of the interface with equilibrium constant K_a, and finally the electrochemically driven transfer of $DPPH^+$(aq) to $DPPH^+$(org). For the chemical steps of the square scheme, the forward and backward rate constants are related by the aforementioned equilibrium constants, and the rate constants for each electrochemical step are given a Butler-Volmer form depending exponentially on $\Delta_o^w\phi$. Given that the stoichiometry of the interfacial-direct and interfacial-sequential electrochemical steps are different, the standard rate constants k^0 have correspondingly different units. To compare the kinetics of either step, an exchange current density j_0 was used to calculate k^0 along with the bulk concentration of all species (**S8**). Accordingly, the following simulations use $j_{0,direct}$ and $j_{0,sequential}$ for comparison.

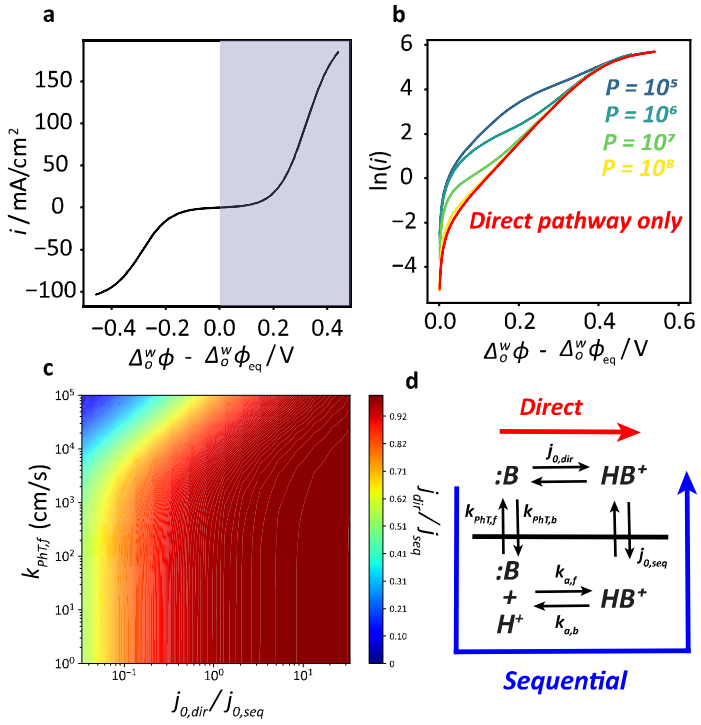

Figure 4 | COMSOL simulations of kinetically limited proton transfer and the influence of the B(org) → B(aq) partition step. (a) Representative CV of kinetically irreversible facilitated proton transfer. (b) Tafel plots of facilitated proton transfer where both direct and sequential mechanisms are operative, and the partition coefficient is varied. The color of the traces corresponds to the partition coefficients shown in the inset, and the red trace is the simulated Tafel plot when only the direct mechanism is operative. (c) The fraction of the total simulated current arising from the direct mechanism as a function of the B(aq)→B(org) phase transfer rate constant $k_{PhT,f}$ and the ratio of the exchange current densities of the direct and sequential pathway. The overpotential was arbitrarily chosen to be 50 mV (d) A square scheme diagram showing the chemical equilibria that comprise interfacial-direct and sequential proton transfer. Above the solid horizontal line is the organic phase, and below is the aqueous phase.

Tafel plots were generated from simulations of fully irreversible CVs (**Figure 4b**). This degree of irreversibility has never been demonstrated experimentally due to extremely fast kinetics for ion transfer at the ITIES and a practical limitation on how small nanopipette orifices can be. However, it can be artificially simulated by forcing the exchange current density in the model to be small relative to the cell's mass transfer coefficient. The resulting current-potential plot (**Figure 4a**) shows classic kinetically irreversible electrochemical behavior, where the exponential rise in current at low overpotentials is purely controlled by electrochemical kinetics, and at larger overpotentials the current levels off as diffusion of species to the

interface becomes rate limiting. To highlight changes in the kinetic regime, the logarithm of the current axis is taken to generate a Tafel plot for the simulated facilitated ion transfer reaction, and the exchange current for the interfacial-direct pathway was forced to be 10 times slower than the interfacial-sequential pathway so that the influence of the partition coefficient could be clearly seen (**Figure 4b**). In this representation, increasing the partition coefficient of the proton acceptor creates a shoulder in the current-potential response, which represents the finite and potential-independent rate of the preceding neutral phase-transfer step. In this scheme, the maximum rate of the partitioning step is proportional to the rate constant for B(org)→ B(aq) transfer $k_{PhT,b}$ which can be equivalently expressed in terms of the B(aq)→ B(org) rate constant and partition coefficient $k_{PhT,f}/P$. When the partition coefficient exceeds 10^8 in this simulation, the Tafel plot for the combined mechanism almost completely overlaps with the Tafel plot of pure interfacial direct transfer, agreeing with the intuition that very hydrophobic molecules will resist aqueous to organic phase transfer, and if an alternative pathway can bypass this energetically uphill intermediate step, it will carry most of the current.

The partition coefficient for DPP was measured to be 10^5 via shake flask experiments (**Figure S2**) and is thus known. However, **Figure 4c** reveals how the fraction of the current carried by the direct mechanism depends on the remaining unknown kinetic parameters in the system while remaining agnostic about the values they should assume, namely the B(aq)→ B(org) partitioning rate constant $k_{PhT,f}$, and the exchange current densities for the individual parallel pathways $j_{0,direct}$ and $j_{0,sequential}$. At an arbitrary overpotential $\eta = 50$ mV, the current arising from the direct pathway was divided by the total current flowing through the interface at varying combinations of $k_{PhT,f}$ and $j_{0,direct}/j_{0,sequential}$ (where $j_{0,sequential}$ was set to be 30 mA/cm^2 to simulate quasireversible kinetic behavior in the system). **Figure 4c** shows that if the kinetics of the direct and sequential electrochemical steps are equal ($j_{0,direct}/j_{0,sequential} = 1$), then $k_{PhT,f}$ can assume a value between 1 to10^5 cm/s and the total current is still mostly carried by the interfacial-direct mechanism, with $j_{direct}/j_{sequential} \approx 0.75$ at the upper end of this range. This arises from the fact that $k_{PhT,f}$ effectively controls the maximum rate that current can

flow through the sequential pathway and thus it can only support a small fraction of the total current drawn from the system when the current demand is high. The direct mechanism does not have such a limitation, so the remainer of the current flows through this pathway instead. It can be seen at the highest value of $k_{PhT,f} = 10^5$ the sequential pathway can meet more of the current demands of the system and thus the fraction $j_{direct}/j_{sequential}$ is somewhat lower. We estimate that the upper bound of a rate constant for a partitioning process should be related to the average velocity of a molecule along its mean free path in solution, which in this case would be on the order of 10^3 cm/s for DPP in liquid water (**S7**). Thus, for a measured partition coefficient of 10^5 the current in a kinetic measurement should be representative of the interfacial direct mechanism, unless the intrinsic kinetics of the direct mechanism ($j_{0,direct}$) is more than an order of magnitude lower than that of the sequential mechanism. Even in this case, the contribution of the sequential mechanism quickly decreases with increasing overpotential (**Figure S5**) and the majority of the current potential response in a kinetic measurement would be reflective of the interfacial direct mechanism.

Poised, equilibrium ion-transfer potential measurements. With the direct PT assignment made in the previous sections from diffusion-limited voltammetry and Multiphysics simulations of interfacial kinetics, DPP was selected as a suitable proton acceptor for further experimental investigation of interfacial proton-transfer kinetics. A conjugate-acid salt of DPP (2,6-diphenylpyridinium tetrakis(3,5-bis(trifluoromethyl)phenyl)borate) was synthesized via a biphasic metathesis reaction reported in literature[32] so that both forms of the "proton-transfer couple" could be initially present in the following nanopipette voltammetry measurement.

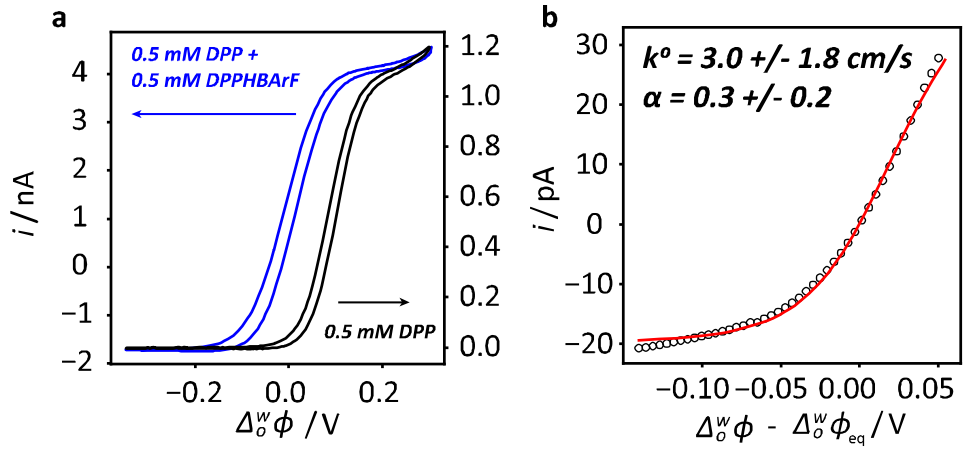

Figure 4 | Voltammetry data with both DPP and DPPH initially present in the organic electrolyte and kinetic measurements at nanopipette interface. Cyclic voltammetry in micropipette electrochemical cell where the TFT electrolyte contains 0.5 mM DPP (a, black) and 0.5 mM DPP + 0.5 mM DPPHBArF (a, blue) revealing the negative limiting current corresponding to the bulk concentration of $DPPH^+$. Averaged cyclic voltammogram with 0.5 mM DPP + 0.5 mM DPPHBArF in the TFT phase (c). The best fit curve of equation 2-4 overlayed in red with best fit values for k^0 and α shown at the top of the graph reported as the average +/- standard deviation of four separate experiments (SI). The radius of the pipette was measured to be 160 nm via SEM.

Figure 4a shows the effect of adding equal amounts of DPP and DPPHBArF to the TFT electrolyte. When only DPP is present, a positive limiting current proportional to the bulk concentration of DPP is observed in the CV around 0.18 V and no current is passed at potentials negative of 0 V in this experiment. In a separate experiment, an equal concentration of DPPHBArF was added to the TFT electrolyte, and a non-zero limiting current was observed negative of 0 V. This limiting current is proportional to the bulk concentration of DPPHBArF, and the difference in the magnitude of positive and negative limiting current is due to the lower diffusion coefficient of $DPPH^+$ in TFT. The point where the steady state voltammogram intersects the potential axis was identified as the equilibrium potential $\Delta_o^w\phi_{eq}$ for that experiment. We found that the equilibrium potential read by the potentiostat is different in every experiment due to the variability of the silver pseudo-reference electrode potential in the TFT electrolyte. Importantly, referencing all other potentials to a particular cell's $\Delta_o^w\phi_{eq}$ allows us to simply analyze current as a function of ion-transfer overpotential rather than an arbitrary pseudo-reference potential.

Subsequently, the same electrolyte composition was used in a nanopipette electrochemical cell for the determination of kinetic values k^0 and α (**Figure 4b**). Equation 2-4 for quasi-reversible steady-state voltammetry was fit to the average of the experimental steady-state voltammogram. This equation is commonly used to fit nanopipette CVs of facilitated ion transfer and assumes that the current is controlled by the concentration of DPP/DPPH+ at the interface, which was achieved experimentally by keeping the pH of the aqueous solution low such that $[H^+]>>[DPP] + [DPPH^+]$. The best fit values for k^0 and α were 3.0 +/- 1.8 cm/s and 0.3 +/- 0.2, respectively. Given that equation 2-4 uses the phenomenological Butler-Volmer kinetic model, the extracted value for α should only be interpreted as the fraction of the overpotential apparently used to drive the forward reaction $H^+(aq) + B(org) \rightarrow HB^+(org)$. Since ion transfer at the liquid-liquid interface is not a one-electron outer-sphere redox reaction, we do not expect α to report on the shape of the activation barrier of the rate-determining charge transfer step.

$$i = -FAm_{DPPH}(C_{DPPH} - \theta C_{DPP})\frac{\kappa}{1+\kappa\theta} \quad (2)$$

$$\theta = 1 + \left(\frac{D_{DPPH}}{D_{DPP}}\right)\exp\left(\frac{zF}{RT}(\Delta_o^w\phi - \Delta_o^w\phi_{eq})\right) \quad (3)$$

$$\kappa = \frac{k_0}{m_{DPPH}}\exp\left(\frac{-\alpha zF}{RT}(\Delta_o^w\phi - \Delta_o^w\phi_{eq})\right) \quad (4)$$

The measured k^0 of ~3 cm/s is comparable to the measured standard rate constant for some types of metal-deposition reactions,[3] and roughly an order of magnitude larger than what has been reported for the $Fe(CN)_6^{3-}/Fe(CN)_6^{4-}$ couple. The k^0 of ~3 cm/s found here, however, should be interpreted as an apparent lower bound on the standard rate constant for proton-transfer at the ITIES given that the fit equation differs very little from the diffusion-limited case (**Figure S6**). It is possible that proton transfer across the ITIES is considerably faster than can be reliably measured by electrochemical methods alone, and given the importance of ion transfer in electrochemistry we should try to explain why this is so.

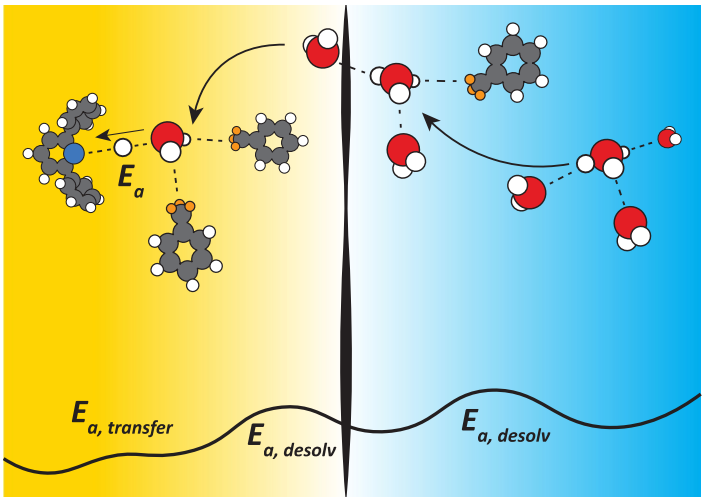

Figure 6 | Proposed molecular picture of proton transfer at the water|TFT interface. Protons experience interactions only with water molecules in the bulk water phase (right), and may partially exchange solvent-shell water with trifluorotoluene in the mixed solvent interphase region as they approach the interface. On the organic side of the interface (left) DPP molecules are present to accept protons. The preceding proton partial-desolvation steps are characterized by sequential activation barriers $E_{a,desolv}$ and the final proton transfer step to DPP by $E_{a,transfer}$. Overall, the kinetics of proton transfer are hypothesized to be controlled by the aggregation of many small partial desolvation steps as it moves through the mixed solvent interphase region.

The use of a relatively polar organic solvent means there are stronger aqueous-nonaqueous interactions at the interface compared to nonpolar solvents like carbon tetrachloride and linear alkanes. In the case of water|1,2-dichloroethane (DCE) systems, this has been shown to produce a boundary resembling more of a mixed solvent interphase.[33] Given similar dipole moments of TFT and DCE (2.86 and 1.86 D, respectively), we assume that the water|TFT system possesses a similar interphase region at the boundary between bulk electrolytes. Water molecules within the water|TFT boundary interphase experience a diverse range of water-water and water-TFT interactions and the range of intermolecular forces may allow for populations of equilibrium "proton-water-TFT" solvation states to smoothly guide the transferring proton along its reaction coordinate.[3] Ion-solvent dynamics thus appear key to understanding PT kinetics in electrochemical systems and beyond. Notably, the role of sequential solvation states along a proton's transit to the electrochemical interface is not described by current microscopic theories of PT, which this work suggests is important in interpreting apparent PT reaction rates. While studying PT is relevant for energy

applications and serves as a testbed for understanding fundamental concepts in electrochemistry, it also serves as a "bridging" model system towards developing a general theory of interfacial ion transfer from foundational concepts provided by Marcus theory. The proton has quantum mechanical character like an electron and may tunnel through the transition state as an electron would, but also has discrete ionic character and interacts with the surrounding solvent as such, thus bearing characteristics we ultimately aim to describe for completely classical particles such as heavy ions like Na^+ relevant in energy storage and biology.

Conclusion

We have demonstrated that micropipette electrochemical cells with radii between 2 and 10 μm can be used to assess whether a lipophilic basic compound is suitable for the study of PT kinetics at the liquid-liquid interface. By switching the position of the electrolyte solutions between the inside and outside of the pipette, asymmetric transport limitations in the cyclic voltammetry revealed that DPP facilitates PT via an interfacial mechanism at an aqueous electrolyte pH of 1. Finite-element simulations of facilitated ion transfer models reveal that both sequential and direct mechanisms may contribute to the measured current, but that increasing the partition coefficient of the simulated proton acceptor reduced the contribution of the sequential current to the overall current response as it lowered the maximum potential-independent rate of neutral phase transfer. The kinetic rate constants of the neutral phase transfer step also affect whether proton transfer will occur via a direct or sequential mechanism, however within the range of physically reasonable values, PT is not likely to proceed through a sequential mechanism. Via nanopipette voltammetry we collected partially activation-controlled PT data which was fit to a model for the extraction of fundamental kinetic parameters k^0 and α. The large value of the obtained standard rate constant > 3 cm/s points to interfacial ionic processes being anomalously fast given the need to exchange solvent molecules around the ion during transit. We hypothesized that the transferring proton must be guided along its reaction coordinate by a gradient in equilibrium solvation states, though further experiments and modeling would be needed to support this claim. Nevertheless, ultrafast ion transfer at the liquid-liquid interface stands as a promising

model system to study ion-solvent interactions in interfacial electrochemical systems in the absence of the usual defects inherent to electrode-electrolyte interfaces. Understanding more about why ion transfer at the ITIES is so fast may yield new insight into ways to accelerate or catalyze ion transfer in systems where it is likely to be rate determining such as battery-type intercalation reactions and electrocatalysis.

Experimental Methods

Electrodes. The AgCl aqueous electrode was prepared via oxidation of Ag wire in 100 mM HCl at a rate of 1 mA for 10 minutes. The nonaqueous pseudoreference electrode was an Ag wire wiped with sandpaper and sonicated in water for several minutes. It was deemed acceptable if the open circuit potential against the aqueous AgCl wire in an ion transfer at the ITIES experiment was stable to within +/ 10 mV.

Pipettes. Pipettes were made by pulling quartz capillaries (ID 0.5 mm, OD 1 mm) in a Sutter P-2000 pipette puller. We used a pulling program with parameters HEAT = 700, FILAMENT = 4, VELOCITY = 10, DELAY = 120, PULL = 60 which typically resulted in 6 pulls before separation. The pipette was immediately inspected under an optical microscope to be sure it was of acceptable quality. Pipettes that did not have a perfectly flat opening were used for experiments, but those that had cracks or slivers of glass protruding from the side were discarded.

Electrolytes. Bis(triphenylphosphine)iminium tetrakis(4-chlorophenyl)borate (BATPBCl) was synthesized by dissolving equal molar amounts of bis(triphenylphosphine)iminium chloride and potassium tetrakis(4-chlorophenyl)borate separately in 2:1 (v/v%) methanol to water solution. The solution of potassium tetrakis(4-chlorophenyl)borate was added dropwise to the bis(triphenylphosphine)iminium chloride solution under fast stirring, and we observed a white precipitate forming immediately. The resulting mixture was left stirring for 1 h, followed by vacuum filtration with a glass frit filter. The resulting paste was removed with a clean plastic scoopula and transferred to another vial with more of the water methanol mixture, then stirred on high speed for 10 min. The filtered precipitate is then transferred to a clean vial and recrystallized in hot ethanol. Once dried in oven overnight, or simply under vacuum, 25 mg

of the resulting powder is dissolved in 5 mL trifluorotoluene to make a nominal 5 mM solution of BATPBCl in TFT. The aqueous electrolyte was made by diluting 12.1 N HCl with 18.2 MΩ cm water to the desired concentration. The bases were made in ~5 mM stock solutions, and then diluted 10x by volume in the supporting electrolyte using analytical micropipette.

Electrochemical measurements. Pipettes were rendered hydrophobic via silanization with trimethylchlorosilane. Outer surfaces of pipettes were immersed in liquid trimethylchlorosilane with a constant flow of N_2 through the pipette for several minutes with rapid bubbling observed at the pipette tip. Following this treatment, the pipette was dried in air under continued flow of nitrogen through the interior. Inner surfaces of pipettes were silanized by drawing liquid trimethylchlorosilane up into the pipette for several minutes. Following treatment, the trimethylchlorosilane was expelled, and the pipette was dried under flowing N_2. The pipettes were filled with electrolyte solutions using a flexible microsyringe. The aqueous solution was dispensed at the top opening of the pipette and allowed to wick down the filament to fill the tip. If one tries to fill the tip directly, then bubbles may form and are difficult to remove. The nonaqueous electrolyte was simply dispensed into the tip and bubbles rarely form or persist if they do. The AgCl electrode was placed in the aqueous solution and the Ag pseudo reference was placed in the nonaqueous solution.

Electrochemical data was collected using a Biologic SP-200 potentiostat with an ultra-low current amplifier. An Ag/AgCl wire in the aqueous phase served as the working electrode and a nonaqueous Ag wire served as the counter and reference, such that the reported $\Delta\phi_o^w$ is always defined as $\phi_{aqueous} - \phi_{nonaqueous} + \phi_{ref}$. Here ϕ_{ref} is the equilibrium potential difference between the Ag/AgCl electrode and the Ag pseudo-reference which were both assumed to act as ideally nonpolarizable electrodes under the nA-pA applied currents. Measurements were collected after the open circuit potential was stable to within $\pm$10 mV of a given value. For cyclic voltametric measurements the working electrode potential was controlled vs the potential of the reference/counter electrode. Oxidation current at the working electrode was defined as positive.

References

(1) Kuo, D.-Y.; Lu, X.; Hu, B.; Abruña, H. D.; Suntivich, J. Rate and Mechanism of Electrochemical Formation of Surface-Bound Hydrogen on Pt(111) Single Crystals. *The Journal of Physical Chemistry Letters* **2022**, *13* (27), 6383-6390. DOI: 10.1021/acs.jpclett.2c01734.
(2) Pinto, L. M. C.; Spohr, E.; Quaino, P.; Santos, E.; Schmickler, W. Why Silver Deposition is so Fast: Solving the Enigma of Metal Deposition. *Angewandte Chemie International Edition* **2013**, *52* (30), 7883-7885, https://doi.org/10.1002/anie.201301998. DOI: https://doi.org/10.1002/anie.201301998 (acccessed 2023/05/08).
(3) Gileadi, E. The enigma of metal deposition. *Journal of Electroanalytical Chemistry* **2011**, *660* (2), 247-253. DOI: https://doi.org/10.1016/j.jelechem.2011.01.025.
(4) Bazant, M. Z. Theory of Chemical Kinetics and Charge Transfer based on Nonequilibrium Thermodynamics. *Accounts of Chemical Research* **2013**, *46* (5), 1144-1160. DOI: 10.1021/ar300145c.
(5) Sood, A.; Poletayev, A. D.; Cogswell, D. A.; Csernica, P. M.; Mefford, J. T.; Fraggedakis, D.; Toney, M. F.; Lindenberg, A. M.; Bazant, M. Z.; Chueh, W. C. Electrochemical ion insertion from the atomic to the device scale. *Nature Reviews Materials* **2021**, *6* (9), 847-867. DOI: 10.1038/s41578-021-00314-y.
(6) Bazant, M. Z. Unified quantum theory of electrochemical kinetics by coupled ion–electron transfer. *Faraday Discussions* **2023**, *246* (0), 60-124, 10.1039/D3FD00108C. DOI: 10.1039/D3FD00108C.
(7) Kiefer, P. M.; Hynes, J. T. Nonlinear Free Energy Relations for Adiabatic Proton Transfer Reactions in a Polar Environment. I. Fixed Proton Donor−Acceptor Separation. *The Journal of Physical Chemistry A* **2002**, *106* (9), 1834-1849. DOI: 10.1021/jp0134244.
(8) Kiefer, P. M.; Hynes, J. T. Nonlinear Free Energy Relations for Adiabatic Proton Transfer Reactions in a Polar Environment. II. Inclusion of the Hydrogen Bond Vibration. *The Journal of Physical Chemistry A* **2002**, *106* (9), 1850-1861. DOI: 10.1021/jp013425w.
(9) Hölzle, M. H.; Zwing, V.; Kolb, D. M. The influence of steps on the deposition of Cu onto Au(111). *Electrochimica Acta* **1995**, *40* (10), 1237-1247. DOI: https://doi.org/10.1016/0013-4686(95)00055-J.
(10) McCrum, I. T.; Chen, X.; Schwarz, K. A.; Janik, M. J.; Koper, M. T. M. Effect of Step Density and Orientation on the Apparent pH Dependence of Hydrogen and Hydroxide Adsorption on Stepped Platinum Surfaces. *The Journal of Physical Chemistry C* **2018**, *122* (29), 16756-16764. DOI: 10.1021/acs.jpcc.8b03660.
(11) McCrum, I. T.; Koper, M. T. M. The role of adsorbed hydroxide in hydrogen evolution reaction kinetics on modified platinum. *Nature Energy* **2020**, *5* (11), 891-899. DOI: 10.1038/s41560-020-00710-8.
(12) Grahame, D. C. The Electrical Double Layer and the Theory of Electrocapillarity. *Chemical Reviews* **1947**, *41* (3), 441-501. DOI: 10.1021/cr60130a002.
(13) Koper, M. T. M. A basic solution. *Nature Chemistry* **2013**, *5* (4), 255-256. DOI: 10.1038/nchem.1600.
(14) Kortlever, R.; Shen, J.; Schouten, K. J. P.; Calle-Vallejo, F.; Koper, M. T. M. Catalysts and Reaction Pathways for the Electrochemical Reduction of Carbon Dioxide. *The Journal of Physical Chemistry Letters* **2015**, *6* (20), 4073-4082. DOI: 10.1021/acs.jpclett.5b01559.
(15) Reece, S. Y.; Nocera, D. G. Proton-Coupled Electron Transfer in Biology: Results from Synergistic Studies in Natural and Model Systems. *Annual Review of Biochemistry* **2009**, *78* (1), 673-699. DOI: 10.1146/annurev.biochem.78.080207.092132 (acccessed 2023/10/11).
(16) Mayer, J. M. PROTON-COUPLED ELECTRON TRANSFER: A Reaction Chemist's View. *Annual Review of Physical Chemistry* **2004**, *55* (1), 363-390. DOI: 10.1146/annurev.physchem.55.091602.094446 (acccessed 2023/10/11).

(17) Weinberg, D. R.; Gagliardi, C. J.; Hull, J. F.; Murphy, C. F.; Kent, C. A.; Westlake, B. C.; Paul, A.; Ess, D. H.; McCafferty, D. G.; Meyer, T. J. Proton-Coupled Electron Transfer. *Chemical Reviews* **2012**, *112* (7), 4016-4093. DOI: 10.1021/cr200177j.
(18) Tyburski, R.; Liu, T.; Glover, S. D.; Hammarström, L. Proton-Coupled Electron Transfer Guidelines, Fair and Square. *Journal of the American Chemical Society* **2021**, *143* (2), 560-576. DOI: 10.1021/jacs.0c09106.
(19) Fang, Y.-H.; Wei, G.-F.; Liu, Z.-P. Catalytic Role of Minority Species and Minority Sites for Electrochemical Hydrogen Evolution on Metals: Surface Charging, Coverage, and Tafel Kinetics. *The Journal of Physical Chemistry C* **2013**, *117* (15), 7669-7680. DOI: 10.1021/jp400608p.
(20) Nørskov, J. K.; Bligaard, T.; Logadottir, A.; Kitchin, J. R.; Chen, J. G.; Pandelov, S.; Stimming, U. Trends in the Exchange Current for Hydrogen Evolution. *Journal of The Electrochemical Society* **2005**, *152* (3), J23. DOI: 10.1149/1.1856988.
(21) Jung, O.; Jackson, M. N.; Bisbey, R. P.; Kogan, N. E.; Surendranath, Y. Innocent buffers reveal the intrinsic pH- and coverage-dependent kinetics of the hydrogen evolution reaction on noble metals. *Joule* **2022**, *6* (2), 476-493. DOI: https://doi.org/10.1016/j.joule.2022.01.007.
(22) Jackson, M. N.; Jung, O.; Lamotte, H. C.; Surendranath, Y. Donor-Dependent Promotion of Interfacial Proton-Coupled Electron Transfer in Aqueous Electrocatalysis. *ACS Catalysis* **2019**, *9* (4), 3737-3743. DOI: 10.1021/acscatal.9b00056.
(23) Gobry, V.; Ulmeanu, S.; Reymond, F.; Bouchard, G.; Carrupt, P.-A.; Testa, B.; Girault, H. H. Generalization of Ionic Partition Diagrams to Lipophilic Compounds and to Biphasic Systems with Variable Phase Volume Ratios. *Journal of the American Chemical Society* **2001**, *123* (43), 10684-10690. DOI: 10.1021/ja015914f.
(24) Reymond, F.; Chopineaux-Courtois, V.; Steyaert, G.; Bouchard, G.; Carrupt, P.-A.; Testa, B.; Girault, H. H. Ionic partition diagrams of ionisable drugs: pH-lipophilicity profiles, transfer mechanisms and charge effects on solvation. *Journal of Electroanalytical Chemistry* **1999**, *462* (2), 235-250. DOI: https://doi.org/10.1016/S0022-0728(98)00418-5.
(25) Reymond, F.; Steyaert, G.; Carrupt, P.-A.; Testa, B.; Girault, H. Ionic Partition Diagrams: A Potential−pH Representation. *Journal of the American Chemical Society* **1996**, *118* (47), 11951-11957. DOI: 10.1021/ja962187t.
(26) Wang, Y.; Velmurugan, J.; Mirkin, M. V. Kinetics of Charge-Transfer Reactions at Nanoscopic Electrochemical Interfaces. *Israel Journal of Chemistry* **2010**, *50* (3), 291-305. DOI: https://doi.org/10.1002/ijch.201000026 (acccessed 2023/10/17).
(27) Wang, Y.; Velmurugan, J.; Mirkin, M. V.; Rodgers, P. J.; Kim, J.; Amemiya, S. Kinetic Study of Rapid Transfer of Tetraethylammonium at the 1,2-Dichloroethane/Water Interface by Nanopipet Voltammetry of Common Ions. *Analytical Chemistry* **2010**, *82* (1), 77-83. DOI: 10.1021/ac902244s.
(28) Rodgers, P. J.; Amemiya, S.; Wang, Y.; Mirkin, M. V. Nanopipet Voltammetry of Common Ions across the Liquid−Liquid Interface. Theory and Limitations in Kinetic Analysis of Nanoelectrode Voltammograms. *Analytical Chemistry* **2010**, *82* (1), 84-90. DOI: 10.1021/ac9022428.
(29) Velázquez-Manzanares, M.; Schiffrin, D. J. Kinetics of facilitated proton transfer by hydrophobic aromatic amines across the water/1,2-dichloroethane interface. *Electrochimica Acta* **2004**, *49* (26), 4651-4658. DOI: https://doi.org/10.1016/j.electacta.2004.05.027.
(30) Benvidi, A.; Lanjwani, S. N.; Ding, Z. Facilitated proton transfer by 2-acetylpyridine-4-phenyl-3-thiosemicarbazone across water/1,2-dichloroethane interface. *Journal of Electroanalytical Chemistry* **2010**, *641* (1), 99-103. DOI: https://doi.org/10.1016/j.jelechem.2009.12.011.
(31) Shao, Y.; Osborne, M. D.; Girault, H. H. Assisted ion transfer at micro-ITIES supported at the tip of micropipettes. *Journal of Electroanalytical Chemistry and Interfacial Electrochemistry* **1991**, *318* (1), 101-109. DOI: https://doi.org/10.1016/0022-0728(91)85297-3.

(32) Pollice, R.; Bot, M.; Kobylianskii, I. J.; Shenderovich, I.; Chen, P. Attenuation of London Dispersion in Dichloromethane Solutions. *Journal of the American Chemical Society* **2017**, *139* (37), 13126-13140. DOI: 10.1021/jacs.7b06997.
(33) Moore, F. G.; Richmond, G. L. Integration or Segregation: How Do Molecules Behave at Oil/Water Interfaces? *Accounts of Chemical Research* **2008**, *41* (6), 739-748. DOI: 10.1021/ar7002732.